

# Possible Universal Limit for Valence Parton Distributions

Christopher Leon, Misak M. Sargsian

*Department of Physics, Florida International University, Miami, FL 33199 USA*

(Dated: February 17, 2023)

We report the observation of the existence of a possible universal limit for valence parton distributions that should exist once partonic degrees of freedom are relevant for high energy scattering from strongly interacting bound systems like a nucleon, meson or a few nucleon system at very short distances. Our observation is based on the notion that the Bjorken  $x$  weighted valence parton distribution function has a peak,  $x_p$ , that characterizes the average momentum fraction carried out by the valence quarks in the system. Within the residual mean-field model of the valence quark distribution we found that  $x_p$  has an upper limit:  $x_p \leq \frac{1}{2(n_V-1)}$ , where  $n_V$  is the number of valence quarks which can be considered in the cluster embedded in the strongly interacting environment of the bound system. The existence of such a limit imposes a new constraint on choosing the starting resolution scale  $Q_0$  for PDFs. Our prediction for the nucleon is that  $x_p|_{Q \rightarrow Q_0} \leq \frac{1}{4}$ , which is in agreement with all the available valence PDFs that employ the standard approach for selecting starting  $Q_0$ . We also demonstrate how the existence of this limit can be used to check the onset of quark-clusters in short range nucleon correlations in nuclei.

## I. INTRODUCTION

Valence quarks are one of the most important constituents of hadrons, defining their baryonic number and representing “effective” fermions interacting mutually and with the hadronic interior. These interactions being non-perturbative pose significant challenges in their description within Quantum Chromodynamics (QCD). One of the quantities representing a testing ground for a non-perturbative QCD description of valence quarks are the partonic distribution functions (PDFs). During the last several decades there have been extensive efforts in the phenomenological extraction of valence PDFs from the analysis of deep inelastic scattering (DIS) from hadronic targets and Drell-Yan processes[1–3]. There are few empirical constraints on the behavior of valence PDFs and possible new constraints are important for the precision of the extraction of PDFs in global analyses. Theoretical modeling of valence PDFs and comparing them with phenomenological PDFs is one direction that allows the introduction of additional constraints, progressing the understanding of the valence structure of hadrons.

Even though the shapes of the valence PDFs are not observables, many theoretical models however predict specific shapes at different ranges of Bjorken  $x$ . The feedback of such modeling is that their predictions are used in constructing the ansatzes for PDF parameterizations. For example, a  $(1-x)^N$  asymptote at large  $x$  is predicted from the quark counting rule, according to which  $N = 2n - 3 + 2|\lambda_h - \lambda_i|$ , where  $n$  is the number of valence quarks and  $\lambda_h$  and  $\lambda_i$  are the helicities of the hadron and struck quark, respectively. Similarly, the  $x^s$  behavior for valence quarks is expected at small  $x$  following from dominance of Regge dynamics with exchanged spin  $s = 0.5$ . Both of these predictions are used in the ansatzes of phenomenological PDFs. In the present work we focus on another unique characteristic of valence PDFs, that is the  $x$ -weighted distribution has a distinguishable peak-like property for all approximation orders, factorization,

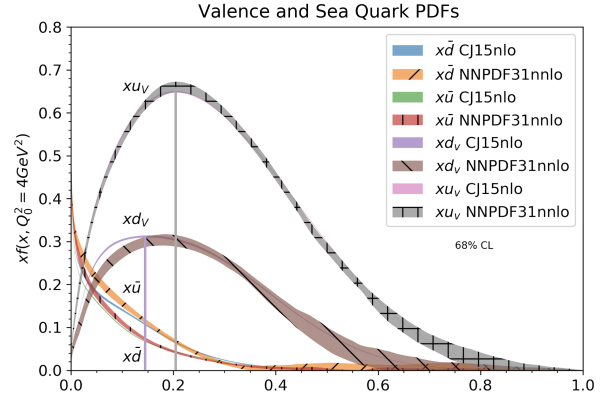


FIG. 1: The valence and sea PDFs for nucleon using the CJ15nlo[2] and NNPDF31nnlo[4] sets evaluated at  $Q_0^2 = 4 \text{ GeV}^2$ . Error bands show the Hessian 68 % confidence level.

and renormalization scales (Fig.1). The QCD evolution shifts the peak position of the distribution at smaller  $x$  values resulting in an interesting correlation between  $x_p$  and the height of the peak in the form[5]:

$$x_p(Q^2) q_V(x_p, Q^2) = h(x_p) = C e^{D x_p(Q^2)}, \quad (1)$$

where  $C$  and  $D$  are constants. At  $Q^2$  large enough that quark degrees of freedom are relevant, and small enough such that the QCD evolution does not shift the peak position substantially towards smaller  $x$ , the peak position within the partonic picture characterizes the average momentum fraction carried by the interacting parton. For the nucleon, the naive expectation (e.g. Ref.[6]) is that  $x_p = \frac{1}{3}$ , indicating that each parton carries one third of the overall longitudinal momentum of the nucleon. Such a result is also expected for a simple non-relativistic constituent quark model. However, a relativistic description of a three-quark system on the Light-Front (LF) deals with more complicated dynamics of momentum sharing between quarks, resulting in, for example [7], a position of the peak at  $x_p = 0.2$  (see Fig.2).

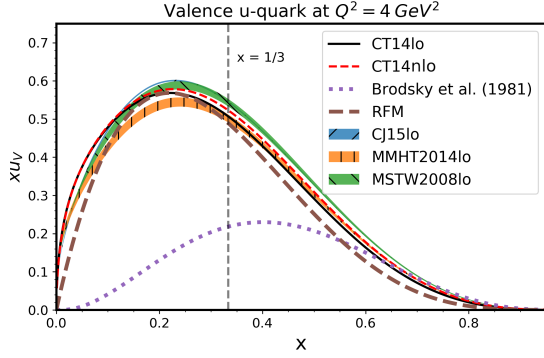


FIG. 2: Peak position of  $xu_V(x)$  distribution compared with prediction of different models calculating valence PDFs.

Moreover, as Fig.1 shows, the position of the peak for valence  $d$  quarks is systematically lower than that of the  $u$ -quarks. To the best of our knowledge this inequality first was addressed within the di-quark model[8–10] in which it was observed that the magnitude of  $x_p$  is related to the mass of the recoil di-quark,  $m_d$ , in the form:  $x_p \approx (1 - \frac{m_d}{m_N})$ . In this picture the empirical observation that  $x_p^d < x_p^u$  follows from the expectation that the vector di-quark being a spectator in the valence  $d$ -quark distribution is heavier than the scalar di-quark for the case of valence  $u$ -quark distribution. In the di-quark model, however, one needs a dynamical model generating masses for di-quarks  $\sim 500 - 700$  MeV/c. In our spectral function approach described in the text, we give a different explanation of this difference based on the difference in masses of the residual systems of hadrons.

This article is arranged as follows: in Sec. II we present a spectral function approach to modeling hadrons, outline the assumptions and derive an expression for the valence PDF in the residual mean-field model. In Sec. III, we present predictions, specifically for  $x_p$  and bound it with an upper limit for all parameterizations. This limit is tested using existing phenomenologically extracted PDFs. Finally, Sec IV contains a summary and outlook. The appendices contain technical calculations and a numerical investigation of  $x_p$  with different parameterizations.

## II. SPECTRAL FUNCTION APPROACH IN DESCRIPTION OF VALENCE QUARK DISTRIBUTIONS

Recently we developed a new approach[12] in which the dynamics of the valence quarks in the nucleon is described through a spectral function framework that distinguishes between the massless valence quark cluster and a residual nucleon system, the latter being characterized by the residual mass distribution  $m_R$ . The model resulted in a prediction that the above discussed peak

position of the valence PDFs are defined according to:

$$x_p = \frac{1}{4} \left( 1 - \frac{m_R}{M_N} \right), \quad (2)$$

where  $M_N$  is the mass of the nucleon. Due to the expected different masses for the residual system, depending on whether the  $u$ - or  $d$ - valence quark is being considered, the model predicted  $x_p^d < x_p^u$  in accordance with empirical data (Fig.1). Another interesting consequence of relation (2) is that it predicts an upper limit of  $x_p^{max} = \frac{1}{4}$ .

To generalize the above relation for any hadron (including also nuclei in the extreme condition of quark-cluster correlations), we present the derivation of partonic distribution function in leading-order approximation for a system consisting of  $n$ - massless valence quark cluster embedded in a strongly interacting bound system.

### A. The valence PDF of a “hadron” containing of $n$ -valence quarks

In the spectral function approach we separate a “hadron” containing of  $n$ -valence quarks into a cluster of  $n$ -valence quarks and a residual system consisting of sea-quarks and gluons (see Fig. 3). In this scenario the valence quarks are embedded in the residual field, thus we refer it as residual mean-field (RMF) model, which was first applied to the case of the nucleon [11, 12]. In the current generalization to the  $n$ -valence quarks the final result, in addition to the nucleon, can be applied to mesons as well as a six-quark system that can be formed due to the strong overlap of two nucleons in the deuteron. Furthermore, by hadron we will also mean strongly overlapped two-nucleon system.

In the current approach rather than taking a full or truncated Fock expansion of the hadron,  $h$ , we model its ket state via:

$$|h\rangle = \psi_{nVq} |nVq\rangle \otimes \psi_{VR} |VR\rangle, \quad (3)$$

where  $\psi_{nVq}$  and  $\psi_{VR}$  are the light-front wave functions (LF) of the  $n$ -valence cluster ( $nVq$ ) and the cluster-residual  $VR$  system, respectively.

Within our framework the LF wave functions can be related to valence PDFs if one calculates the  $F_2(x, Q^2)$  structure function that enters in the cross section of deep inelastic scattering (DIS),  $eh \rightarrow e'X$ . We consider this reaction in the Drell-Yan-West reference frame

$$\begin{aligned} p^\mu &= (p^+, p^-, \mathbf{p}^\perp) = \left( p^+, \frac{m_H^2}{p^+}, \mathbf{0}_\perp \right), \\ q^\mu &= (q^+, q^-, \mathbf{q}^\perp) = \left( 0, \frac{2p^+ \cdot q}{p^+}, \mathbf{q}_\perp \right), \end{aligned} \quad (4)$$

where  $p^\mu$  and  $q^\mu$  are four-momenta of the incoming hadron and virtual photon in light cone (LC) co-

ordinates, with  $Q^2 = -q^2 = |\mathbf{q}_\perp|^2$ ,  $x = \frac{Q^2}{2p \cdot q}$  and  $m_H$  being the mass of the hadron.

The hadronic tensor is given by:

$$W^{\mu\nu}(x, Q^2) = \frac{1}{4\pi m_H} \sum_{q, h_i} \int \delta(k_R^2 - m_R^2) \frac{d^4 k_R}{(2\pi)^3} \\ \times \delta(k_1'^2 - m_1^2) \frac{d^4 k_1'}{(2\pi)^3} \prod_{i=2}^{n_V} \delta(k_i^2 - m_i^2) \frac{d^4 k_i}{(2\pi)^3} \\ \times (2\pi)^4 \delta^{(4)}(P + q - k_1' - \sum_{i=2}^{n_V} k_i - k_R) A^{\mu\dagger} A^\nu, \quad (5)$$

where the amplitude,  $A^\mu$ , is that of the scattering process depicted in Fig. 3. Here,  $k_i^\mu$ ,  $m_i$  and  $h_i$  are 4-momentum, mass, and helicity respectively, with the  $i$  index denoting the valence quarks from  $i = 1, 2, \dots, n_V$ , with  $i = 1$  being the struck quark before interacting with the photon and  $i = 1'$  denoting it after. The index  $i = R, V$  label the residual and valence subsystem, respectively.

The Lorentz invariant phase space for a single particle in light front co-ordinates is:

$$\delta(k^2 - m^2) d^4 k = \frac{dx d^2 \mathbf{k}_\perp}{2x} \Big|_{k^- = \frac{k_\perp^2 + m^2}{k^+}}. \quad (6)$$

In the Bjorken limit,  $Q^2 \rightarrow \infty$  with  $x = \frac{Q^2}{2p \cdot q}$  fixed:

$$\delta^{(4)}(P + q - k_1' - \sum_{i=2}^{n_V} k_i - k_R) \\ = \frac{x_1}{p_N \cdot q} \delta(x_1 - x) \delta\left(1 - x_1 - \sum_{i=2}^{n_V} x_i - x_R\right) \\ \times \delta^{(2)}\left(\sum_{i=1}^{n_V} \mathbf{k}_{i,\perp} + \mathbf{k}_{R,\perp}\right). \quad (7)$$

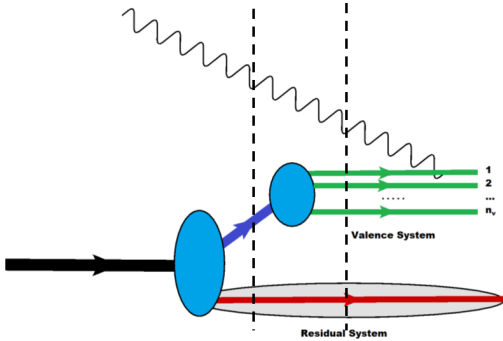


FIG. 3: Light cone time ordered diagram of DIS. Intermediate states are identified by the vertical dashed lines.

For the calculation of the amplitude  $A^\mu$  in Ref[12] we developed effective light-front diagrammatic rules in which we introduced LFWFs through the phenomenolog-

ical vertices and light-front energy denominators in the same form which enters in LF equation of bound states. For the n-valence cluster ( $n_V q$ ) and cluster-residual system (VR) LFWFs are defined as:

$$\psi_{VR}(x_V, \mathbf{k}_{R,\perp}, x_R, \mathbf{k}_{V,\perp}) = \frac{\bar{\chi}_V \bar{\chi}_R \Gamma^{h \rightarrow VR} \chi_h}{m_h^2 - \frac{k_{V,\perp}^2 + m_V^2}{x_V} - \frac{k_{R,\perp}^2 + m_R^2}{x_R}} \\ \psi_{n_V q}(\{\beta_i, \mathbf{k}_{i,\perp}, h_i\}_{i=1}^{n_V}) = \frac{\prod_{i=1}^{n_V} \bar{u}(k_i, h_i) \Gamma^{V \rightarrow n_V q} \chi_V}{m_V^2 - \sum_{i=1}^{n_V} \frac{k_{i,\perp}^2 + m_i^2}{\beta_i}}, \quad (8)$$

where  $(x_V, k_{V,\perp})$  and  $(x_R, k_{R,\perp})$  characterize LC momenta of the cluster and the residual system and  $\{\beta_i, \mathbf{k}_{i,\perp}, h_i\}_{i=1}^{n_V}$  denotes the LC momenta and helicities of the n-valence quarks in the cluster. In the above defined LFWFs  $\Gamma^{h \rightarrow VR}$  and  $\Gamma^{V \rightarrow n_V q}$  are phenomenological vertices describing the transition of the hadron to the cluster-residual system and the valence cluster to n-valence quarks. These vertices absorb all the complexities of LFWs (for example null-modes) that in principle could be calculated in an almost infinite number coupled channel equation for LF Fock state wave functions (see e.g. Ref.[19]). In our approach these wave functions are found phenomenologically by parameterizing them and then verifying their parameters in different QCD processes in which the same LFWFs enter.

In leading order we can relate the amplitude to the LFWFs as follows:

$$A^\mu = \sum_{h_1, h_V} \bar{u}(k_1', h_1') (ie_1 \gamma^\mu) u(k_1, h_1) \frac{\psi_{VR}}{x_V} \frac{\psi_{n_V q}}{\beta_1}. \quad (9)$$

Here  $e_1$  is the charge of quark  $i = 1$ . The LFWFs have dependencies of:

$$\psi_{VR} = \psi_{VR}(x_V, \mathbf{k}_{R,\perp}, x_R, \mathbf{k}_{V,\perp}) \quad (10)$$

$$\psi_{n_V q} = \psi_{n_V q}(\{\beta_i, \tilde{\mathbf{k}}_{i,\perp}, h_i\}_{i=1}^{n_V}) \quad (11)$$

where

$$\tilde{\mathbf{k}}_{i,\perp} = \mathbf{k}_{i,\perp} - \frac{x_i}{x_V} \mathbf{k}_{V,\perp}, \quad (12)$$

$$\beta_i = \frac{x_i}{x_V} \quad (i = 1, \dots, n_V). \quad (13)$$

Eq. 9 simplifies for  $\mu = +$ , resulting in

$$A^+ = 2ie_1 \sum_{h_1, h_V} \psi_{VR} \psi_{n_V q}. \quad (14)$$

In the considered reference frame we can relate the second structure function to the hadronic tensor:

$$F_2(x, Q^2) = \frac{m_H(p \cdot q)}{(p^+)^2} W^{++} = \frac{m_H Q^2}{2x(p^+)^2} W^{++}. \quad (15)$$

The non-negativity condition on the ‘+’ momentum in Eq.(4) eliminates the vacuum contribution where the photon fluctuates into a quark/anti-quark pair,  $\gamma^* \rightarrow q\bar{q}$ . Substituting Eq.’s (6), (7) and (14) into  $W^{++}$  in Eq. (5), from Eq. (15) one obtains:

$$F_2(x) = \sum_q \sum_{h_i} \int^{Q^2} [dx]_{n_V+R} [d^2\mathbf{k}_\perp]_{n_V+R} \times e_q^2 x_1 \delta(x_1 - x) |\psi_{3q}|^2 |\psi_V|^2, \quad (16)$$

where

$$[dx]_{n_V+R} = \prod_{i=1, \dots, n_V, R} \frac{dx_i}{x_i} \delta \left( 1 - \sum_{i=1, \dots, n_V, R} x_i \right) \quad (17)$$

$$[d^2\mathbf{k}_\perp]_{n_V+R} = \prod_{i=1, \dots, n_V, R} \frac{d^2\mathbf{k}_{i,\perp}}{16\pi^3} 16\pi^3 \delta^{(2)} \left( \sum_{i=1, \dots, n_V, R} \mathbf{k}_{i,\perp} \right). \quad (18)$$

Using the leading order relation of  $F_2(x, Q^2) = \sum_i e_i^2 x f_i(x, Q^2)$ , one can then relate the valence PDF through the LFWFs as follows:

$$f_q(x) = \sum_{h_i} \int^{Q^2} [dx]_{n_V+R} [d^2\mathbf{k}_\perp]_{n_V+R} \times \delta(x_1 - x) |\psi_{n_V q}|^2 |\psi_V|^2. \quad (19)$$

Using  $\tilde{\mathbf{k}}_{i,\perp}$  for the valence quarks allows us to factorize the transverse integral:

$$f(x) = \int [dx]_{n_V+R} \delta(x_1 - x) \times \int^{\tilde{Q}_{max}^2} [d^2\tilde{\mathbf{k}}_\perp]_{n_V} \left| \psi_{n_V q}(\{\beta_i, \tilde{\mathbf{k}}_{i,\perp}, h_i\}_{i=1}^{n_V}) \right|^2 \times \int^{Q_{VR,max}^2} \frac{d^2\mathbf{k}_{R,\perp}}{16\pi^3} |\psi_{VR}(x_V, \mathbf{k}_{R,\perp}, x_R, \mathbf{k}_{V,\perp})|^2 \quad (20)$$

where:

$$[d^2\tilde{\mathbf{k}}_\perp]_{n_V} = 16\pi^3 \delta^{(2)} \left( \sum_{i=1}^{n_V} \tilde{\mathbf{k}}_{i,\perp} \right) \prod_{i=1}^{n_V} \frac{d^2\tilde{\mathbf{k}}_{i,\perp}}{16\pi^3} \\ \tilde{\mathbf{k}}_{i,\perp} = \mathbf{k}_{i,\perp} - \frac{x_i}{x_V} \mathbf{k}_{V,\perp}, \quad \beta_i = \frac{x_i}{x_V} \quad (i = 1, \dots, n_V) \quad (21)$$

## B. Valence PDF with Light Front Harmonic Oscillator LFWFs

From the fact that the hadron is a bound, relativistic object we model  $\psi_{n_V q}$  through the mutually coupled relativistic harmonic light-front wave functions[12], to ac-

count the effect of confinement. For  $\psi_{VR}$ , we use a Gaussian function with non-relativistic kinematics used to estimate the  $z$  component of momentum.

$$\psi_{n_V q} = 16\pi^3 m_H A_R \exp \left[ -\frac{B_V}{8} \sum_{i=1}^{n_V} \frac{\tilde{k}_{i,\perp}^2 + m_i^2}{\beta_i} \right] \times e^{\frac{n^2 m^2 B_V}{8}} \sqrt{x_2 \dots x_{n_V}} \quad (22)$$

$$\psi_{VR} = \sqrt{16\pi^3 m_H A_V s} \times \exp \left[ -\frac{B_R}{2} \left( (m_H x_R - m_R)^2 k_{R,\perp}^2 \right) \right] \sqrt{x_R}. \quad (23)$$

Inserting the above wave functions into Eq.(20) one obtains :

$$f(x) = (16\pi^3 m_H)^5 |A_R A_V|^2 e^{\frac{n^2 m^2 B_V}{8}} \times \int [dx]_{n_V+R} \delta(x_1 - x) x_2 \dots x_n \times \int^{\tilde{Q}_{max}^2} [d^2\tilde{\mathbf{k}}_\perp]_{n_V} e^{-\frac{B_V}{4} \sum_i \frac{\tilde{k}_{i,\perp}^2 + m_i^2}{\beta_i}} \times \int^{Q_{VR,max}^2} \frac{d^2\mathbf{k}_{R,\perp}}{16\pi^3} |\psi_{VR}|^2. \quad (24)$$

Taking the  $Q^2 \rightarrow \infty$  limit (see Appendix A) results in :

$$\int [d^2\tilde{\mathbf{k}}_\perp]_{n_V} e^{-\frac{B_V}{4} \sum_i \frac{\tilde{k}_{i,\perp}^2 + m_i^2}{\beta_i}} = \frac{e^{-\frac{B_V}{4} \sum_i \frac{m_i^2}{\beta_i}}}{(16\pi^2)^{n_V-1} (B_V/4)^{n_V-1}} \frac{x_1 x_2 \dots x_{n_V}}{x_V^{n_V}}. \quad (25)$$

Similarly, for the residual transverse integral:

$$\int \frac{d^2\mathbf{k}_{R,\perp}}{16\pi^3} |\psi_{VR}|^2 \quad (26)$$

$$= \frac{\pi e^{-B_R m_H^2 (x_R - \mu_R)^2} x_R}{16\pi^3} \int dk_{R,\perp}^2 e^{-B_R k_{R,\perp}^2} \\ = \frac{e^{-B_R m_H^2 (x_R - \mu_R)^2} x_R}{16\pi^2 B_R}, \quad (27)$$

where  $\mu_R = \frac{m_R}{m_H}$ . Inserting Eq. (25) and (27) into Eq. (24) for the valence PDF one obtains:

$$f(x) = \mathcal{N}_{n_V} \int [dx]_{n_V+R} \times \delta(x_1 - x) \frac{x_1 x_2 \dots x_{n_V}}{x_V^{n_V}} e^{-B_R m_H^2 (x_R - \mu_R)^2} x_R, \quad (28)$$

where

$$\mathcal{N}_{n_V} = \frac{(16\pi^3 m_H)^5 4^{n_V-1} |A_R A_V|^2}{(16\pi^2)^{n_V} B_V^{n_V-1} B_R} e^{\frac{B_V n_V^2 m^2}{4}}. \quad (29)$$

This can be simplified (see Appendix B) to obtain:

$$f(x) = \frac{\mathcal{N}_{n_V}}{(2n_V - 3)!} \times \int_0^{1-x} dx_R \frac{(1 - x_R - x)^{2n-3}}{(1 - x_R)^n} e^{-B_R m_H^2 (x_R - \frac{m_R}{m_H})^2}. \quad (30)$$

### III. ANALYTIC PREDICTIONS OF THE MODEL

Obtained in Eq.(30) expression uses a coupled  $n_V$ -dimensional harmonic oscillator on the Light-Front which does not contain the hard component, which can be generated through the hard gluon exchanges between valence quarks. With such a “soft” wave function one expects that the model has more validity at moderate  $x$  relevant to the peak position of the  $x$  weighted valence PDF distribution (see Fig.1 and Ref.[5]). We expect our model to underestimate the high  $x$  part of the valence PDFs if they are dominated by hard interactions between valence quarks[21].

Our procedure for the case of the nucleon[5] was to fit the height and the position of the  $x$ -weighted valence PDF peak and thereby to evaluate parameters entering the LFWFs of Eq.(8). Once these parameters are fixed then one can use the same wave functions in the calculation of different QCD “objects” like form-factors, generalized partonic distributions or transversities that can be accessed experimentally. This allows us to verify the universalities of LFWFs for multitude of processes at moderate range of  $x \sim 0.1 - 0.4$ .

In the present work we focus on analytic features of the model that does not require a fitting. For this, one observes that for moderate  $x$ , using the exponent in the integrand in Eq.(30) we can evaluate it at its minimum,  $x_R \sim 1 - \frac{m_R}{m_H}$ , resulting in:

$$f(x) \approx \frac{\mathcal{N}_{n_V}}{(2n_V - 3)!(1 - \mu_R)^{n_V}} (1 - x - \mu_R)^{2n_V-3}. \quad (31)$$

The derivation of the approximation in Eq. (31) utilizes the saddle point approximation, which has a correction of  $\mathcal{O}(\frac{1}{B_R m_H^2})$ . Values of  $B_R m_H^2$  extracted from fits to phenomenologically derived proton valence PDFs are typically  $\sim 10 - 50$  [12]. Using Eq. (31) one can calculate the position of the peak of  $x f(x)$  to obtain:

$$x_p = \frac{1}{2(n_V - 1)} \left( 1 - \frac{m_R}{m_H} \right). \quad (32)$$

By the evolution of the DGLAP equations, there is a dependence on  $x_p$  on  $Q^2$ . While there is no exact prescription as to what minimal  $Q_0^2$  to use, one expects it to be large enough for factorization and pQCD to be valid and small enough so that the exact characteristics of the

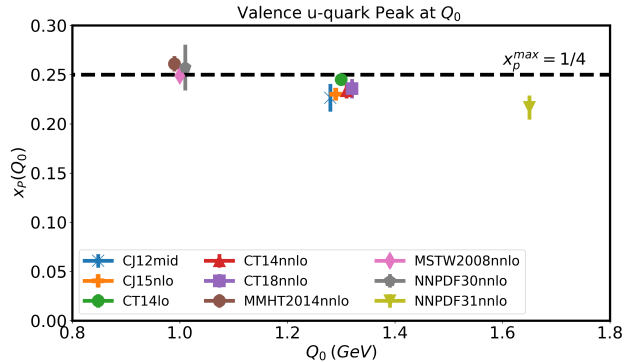


FIG. 4: The up valence peak for various PDFs sets at their starting  $Q_0$  [1–4, 13–16].

residual structure are not important. However, once fixed at a particular  $Q^2$  their renormalization flow is uniquely determined.

Since the mass of the residual system,  $m_R$ , is positive the above equation results in a universal upper limit of the peak position of valence quark PDFs of the form:

$$x_p \leq \frac{1}{2(n_V - 1)}. \quad (33)$$

This upper bound is valid for all  $Q^2$ . A numerical investigation into the validity of Eq. (32) and (33) can be found in Appendix D, where both are found to generally hold for the parameters explored.

For the nucleon this results in Eq.(2) and an upper limit of  $x_p^{max} = \frac{1}{4}$ . This allows us to state that if the partonic degrees are resolved in the nucleon then the position of the peak of the  $x$  weighted valence PDFs should not exceed  $\frac{1}{4}$ . To check this observation, in Fig.4 we compare the results from several valence PDFs at starting  $Q_0$ . Note that only those PDFs are chosen that apply the standard approach in defining starting  $Q_0$ , that is, it assumes the onset of partonic degrees of freedom in the nucleon. The figure shows that at the lowest possible starting  $Q_0 = 1$  GeV (for which partonic degrees of freedom can only start to be relevant) the position of the peak is in agreement with the predicted upper limit of  $\frac{1}{4}$ . For all  $Q > Q_0$  the peak position is less than  $\frac{1}{4}$ , thus satisfying inequity (33). Note that this result is independent on the form of the ansatz in empirical PDF parameterizations. One may think that  $x_p^{max} = \frac{1}{4}$  can be a simple reflection that, in  $m_R \rightarrow 0$  limit the model becomes like a four-massless—body problem. If this is the case, then mesons will correspond to three-massless-body problem expecting  $x_p^{max} = \frac{1}{3}$ . However, as Eq.(33) shows for mesons the model predicts  $x_p < \frac{1}{2}$ , which is in agreement with available pion PDFs[17, 18]. Thus, the result is due to a nontrivial light-cone momentum sharing between valence quarks and residual system.

It is interesting that for the case of 6q-system the model predicts  $x_p < \frac{1}{10}$ , which should be compared to  $\frac{1}{8}$  that follows from the convolution model in which two nucleons in the deuteron did not merge into a 6q state.

Thus, the shift of the peak position towards lower  $x$  reaching to  $\frac{1}{10}$  for the deuteron valence PDFs at fixed  $Q^2$  with increase of internal momentum in the deuteron will indicate the transition from NN to 6q state.

Furthermore, without fixing parameters of the LF wave functions we can calculate the analytic form of the valence PDFs at  $x \rightarrow 1$ . Substituting  $x \rightarrow 1 - \epsilon$  we calculate the integral in Eq.(30) in the small  $\epsilon$  limit, resulting in:

$$f(x) = \frac{\mathcal{N}_{n_V}}{(2n_V - 3)!} e^{-B_R m_H^2 (1 - \mu_R)^2} (1 - x)^{2n_V - 2}. \quad (34)$$

The above relation predicts  $(1 - x)^4$  behavior for nucleon valence PDFs at  $x \rightarrow 1$ , which should be compared with  $(1 - x)^3$  that follows from perturbative QCD arguments that require two hard gluon exchanges between three valence quarks[21]. It is interesting that for mesons one obtains  $(1 - x)^2$ , which is the same as the prediction from pQCD. This indicates that the observation of  $(1 - x)^2$  behavior of the pion valence PDF may not necessarily indicate the dominance of the hard component in the pion wave function. This observation is in agreement with that of [20]. The same is true for the deuteron in which case Eq.(34) predicts  $(1 - x)^{10}$  the same behavior as predicted within pQCD[21].

#### IV. SUMMARY AND OUTLOOK

We introduced a residual field approach in the calculation of valence PDFs of a hadron containing  $n_V$ -valence

quarks. In the approach we describe a hadron as consisting of an  $n_V$ -valence cluster embedded in the residual system of the hadron. Phenomenological LF wave functions are introduced, which do not contain a hard component and the calculation is done within the effective light-front diagrammatic method. Analyzing analytic features of the calculated valence PDFs we predict that there is a universal upper limit for the peak position of the  $x$ -weighted valence PDFs. Namely, for the nucleon we predict an upper limit for  $x_p^{max} = \frac{1}{4}$ , which is in agreement with the all available phenomenological PDFs. This result in our view is non trivial considering that only three-valence quarks exist in the nucleon. One obtains also  $x_p^{max} = \frac{1}{2}$  and  $x_p^{max} = \frac{1}{10}$  for meson and six-quark system respectively.

In discussing the high  $x$  behavior of the PDFs one observes that soft LFWFs predict a faster drop-off for the nucleon PDFs than that of pQCD, while the prediction for pion and the deuteron PDFs are the same as the pQCD prediction.

It will be interesting if the future studies of valence PDFs, both experimentally and on the lattice, could verify the existence of the universal upper limit for the nucleon  $x_p^{max} = \frac{1}{4}$ . Such a position of the peak will be an indicator of the onset of partonic degrees of freedom in the nucleon.

**Acknowledgment:** This work is supported by United States Department of Energy grant under contract DE-FG02-01ER41172

- 
- [1] T. J. Hou *et al.*, arXiv:1912.10053 [hep-ph].
  - [2] A. Accardi, L. T. Brady, W. Melnitchouk, J. F. Owens and N. Sato, Phys. Rev. D **93**, no. 11, 114017 (2016).
  - [3] S. Dulat *et al.*, Phys. Rev. D **93**, no. 3, 033006 (2016).
  - [4] R. D. Ball *et al.* [NNPDF], Eur. Phys. J. C **77**, no.10, 663 (2017) doi:10.1140/epjc/s10052-017-5199-5 [arXiv:1706.00428 [hep-ph]].
  - [5] C. Leon, M. M. Sargsian and F. Vera, MDPI Physics **3**, no.4, 913-923 (2021) doi:10.3390/physics3040057 [arXiv:2003.12902 [hep-ph]].
  - [6] F. Halzen and A. D. Martin, "QUARKS AND LEPTONS: AN INTRODUCTORY COURSE IN MODERN PARTICLE PHYSICS,"
  - [7] S. J. Brodsky, T. Huang and G. P. Lepage, Conf. Proc. C **810816**, 143-199 (1981) SLAC-PUB-16520.
  - [8] F. E. Close and A. W. Thomas, Phys. Lett. B **212**, 227-230 (1988) doi:10.1016/0370-2693(88)90530-8
  - [9] C. D. Roberts, R. J. Holt and S. M. Schmidt, Phys. Lett. B **727**, 249-254 (2013) doi:10.1016/j.physletb.2013.09.038 [arXiv:1308.1236 [nucl-th]].
  - [10] Y. Lu, L. Chang, K. Raya, C. D. Roberts and J. Rodríguez-Quintero, [arXiv:2203.00753 [hep-ph]].
  - [11] C. Leon and M. Sargsian, PoS **LC2019**, 056 (2020) doi:10.22323/1.374.0056 [arXiv:2001.03672 [hep-ph]].
  - [12] C. Leon and M. Sargsian, Eur. Phys. J. C **82**, no.4, 309 (2022) doi:10.1140/epjc/s10052-022-10243-x [arXiv:2012.14030 [hep-ph]].
  - [13] J. F. Owens, A. Accardi and W. Melnitchouk, Phys. Rev. D **87**, no.9, 094012 (2013) doi:10.1103/PhysRevD.87.094012 [arXiv:1212.1702 [hep-ph]].
  - [14] L. A. Harland-Lang, A. D. Martin, P. Motylinski and R. S. Thorne, Eur. Phys. J. C **75**, no.5, 204 (2015) doi:10.1140/epjc/s10052-015-3397-6 [arXiv:1412.3989 [hep-ph]].
  - [15] A. D. Martin, W. J. Stirling, R. S. Thorne and G. Watt, Eur. Phys. J. C **63**, 189-285 (2009) doi:10.1140/epjc/s10052-009-1072-5 [arXiv:0901.0002 [hep-ph]].
  - [16] R. D. Ball *et al.* [NNPDF], JHEP **04**, 040 (2015) doi:10.1007/JHEP04(2015)040 [arXiv:1410.8849 [hep-ph]].
  - [17] P. C. Barry, N. Sato, W. Melnitchouk and C. R. Ji, Phys. Rev. Lett. **121**, no.15, 152001 (2018) doi:10.1103/PhysRevLett.121.152001 [arXiv:1804.01965 [hep-ph]].
  - [18] P. C. Barry *et al.* [Jefferson Lab Angular Momentum (JAM)], Phys. Rev. Lett. **127**, no.23, 232001 (2021) doi:10.1103/PhysRevLett.127.232001 [arXiv:2108.05822]

- [hep-ph]].
- [19] S. J. Brodsky, H. C. Pauli and S. S. Pinsky, Phys. Rept. **301**, 299-486 (1998) doi:10.1016/S0370-1573(97)00089-6 [arXiv:hep-ph/9705477 [hep-ph]].
- [20] A. Efremov and A. Radyushkin, Mod. Phys. Lett. A **24**, 2803-2824 (2009) doi:10.1142/S0217732309001029 [arXiv:0911.1195 [hep-ph]].
- [21] S. J. Brodsky and G. R. Farrar, Phys. Rev. D **11**, 1309 (1975) doi:10.1103/PhysRevD.11.1309

## Appendix A: General Case for Transverse Integral

LF relativistic harmonic oscillators were used in modelling the LFWFs. In integrating over the transverse momentum we will have integrals of the form,

$$I_{n_V} = \int \prod_{j=1}^{n_V} [d^2 \tilde{\mathbf{k}}_{j,\perp}] \exp \left[ - \sum_{j=1}^{n_V} B_j \frac{\tilde{k}_{j,\perp}^2}{x_j} \right]. \quad (\text{A1})$$

We now take  $Q^2 \rightarrow \infty$  in the integral bounds. The  $\tilde{k}_x$  and  $\tilde{k}_y$  integrals are identical, thus we can take it as the square of an  $n_V$ -dimensional integral:

$$\begin{aligned} I_{n_V} &= \int \prod_{j=1}^{n_V} \frac{d^2 \tilde{k}_{j,\perp}}{16\pi^3} 16\pi^3 \delta^{(2)} \left( \sum_{j=1}^{n_V} \tilde{\mathbf{k}}_{j,\perp} \right) \\ &\times \exp \left[ - \sum_{j=1}^{n_V} B_j \frac{\tilde{k}_{j,\perp}^2}{x_j} \right] \\ &= \frac{1}{(16\pi^3)^{n_V-1}} \left( \int \prod_{j=1}^{n_V} d\tilde{k}_j \delta \left( \sum_{j=1}^{n_V} \tilde{k}_j \right) \exp \left[ - \sum_{j=1}^{n_V} B_j \frac{\tilde{k}_j^2}{x_j} \right] \right)^2. \end{aligned} \quad (\text{A2})$$

Now, we make use of the fact that we can take a Fourier decomposition of Dirac delta:  $\delta(\sum_{j=1}^N \tilde{k}_i) = \frac{1}{2\pi} \int_{-\infty}^{\infty} dz e^{iz(\sum_{j=1}^N \tilde{k}_i)}$  in the above equation obtaining,

$$\begin{aligned} I_{n_V} &= \frac{1}{(16\pi^3)^{n_V-1}} \\ &\times \left( \frac{1}{2\pi} \int_{-\infty}^{\infty} dz \prod_{j=1}^{n_V} \int_{-\infty}^{\infty} dk_j \exp \left[ izk_j \right] \exp \left[ - B_j \frac{k_j^2}{x_j} \right] \right)^2. \end{aligned}$$

The integral in the product is just a Fourier transform of a Gaussian. Using the relation  $\int_{-\infty}^{\infty} dx e^{-\alpha x^2} e^{i\omega x} =$

$\sqrt{\frac{\pi}{\alpha}} e^{-\frac{\omega^2}{4\alpha}}$  in the above equation, one obtains:

$$\begin{aligned} I_{n_V} &= \frac{1}{(16\pi^3)^{n_V-1}} \\ &\times \left( \frac{1}{2\pi} \int_{-\infty}^{\infty} dz e^{-z^2 (\sum_{j=1}^{n_V} \frac{x_j}{4B_j})} \prod_{j=1}^{n_V} \sqrt{\frac{\pi x_j}{B_j}} \right)^2 \\ &= \frac{1}{(16\pi^3)^{n_V-1}} \left( \frac{1}{2\pi} \sqrt{\frac{\pi}{\sum_{j=1}^{n_V} \frac{x_j}{4B_j}}} \prod_{j=1}^{n_V} \sqrt{\frac{\pi x_j}{B_j}} \right)^2. \end{aligned}$$

. Thus,

$$I_{n_V} = \frac{1}{(16\pi^3)^{n_V-1}} \frac{(\pi)^{n_V-1}}{\sum_{j=1}^{n_V} \frac{x_j}{B_j}} \prod_{j=1}^{n_V} \frac{x_j}{B_j}. \quad (\text{A3})$$

In Eq. (25) the fact the  $B_j$ 's were the same for all  $i$  and that  $\sum_i \beta_i = 1$  was used.

## Appendix B: The $\mathbf{x}$ Integration of PDFs

Starting at Eq. (28) we use  $x_V = 1 - x_R$  and making the  $[dx]_{n_V+R}$  term explicit:

$$\begin{aligned} f(x) &= \mathcal{N}_{n_V} \int dx_1 \dots dx_{n_V} dx_R \delta \left( 1 - x_R - \sum_{i=1}^{n_V} x_i \right) \\ &\times \delta(x_1 - x) \frac{x_2 \dots x_{n_V}}{(1 - x_R)^{n_V}} e^{-B_R m_H^2 (x_R - \mu_R)^2}. \end{aligned} \quad (\text{B1})$$

The Dirac delta is taken to set  $x_1$  to  $x$ :

$$\begin{aligned} f(x) &= \mathcal{N}_{n_V} \int_0^{1-x} dx_R \int_0^{1-x-x_R} dx_2 \dots \\ &\times \int_0^{1-x-x_R-\sum_{i=2}^{n_V-1} x_i} dx_{n_V} \frac{x_2 \dots x_n}{(1 - x_R)^{n_V}} e^{-B_R m_H^2 (x_R - \mu_R)^2} \\ &\times \delta \left( 1 - x_R - x - \sum_{i=2}^{n_V} x_i \right). \end{aligned} \quad (\text{B2})$$

Now, let  $y_i$  be the relative momentum fraction for the  $i = 2, \dots, n_V$  subsystem:

$$y_i = \frac{x_i}{x_2 + x_3 + \dots + x_{n_V}} = \frac{x_i}{1 - x_R - x} \quad (\text{B3})$$



Doing so, the integral factorizes,

$$\begin{aligned}
f(x) &= \mathcal{N}_{n_V} \int_0^{1-x} dx_R \frac{e^{-B_R m_H^2 (x_R - \mu_R)^2}}{(1-x_R)^{n_V}} \int_0^1 dy_2 y_2 \dots \\
&\int_0^{1-\sum_{i=2}^{n_V-1} y_i} dy_{n_V} y_{n_V} \frac{(1-x_R-x)^{2(n_V-1)}}{(1-x_R)^{n_V}} \\
&\times \delta\left(1-x_R-x-\sum_{i=2}^{n_V} y_i (1-x-x_R)\right) \\
&= \mathcal{N}_{n_V} J_{n_V} \int_0^{1-x} dx_R \frac{(1-x_R-x)^{2n_V-3}}{(1-x_R)^{n_V}} e^{-B_R m_H^2 (x_R - \mu_R)^2},
\end{aligned} \tag{B4}$$

where  $J_{n_V}$  is a constant independent of  $x_R$  and  $x$ . One can show  $J_{n_V} = \frac{1}{(2n_V-3)!}$  (see Appendix C). Thus,

$$\begin{aligned}
f(x) &= \frac{\mathcal{N}_{n_V}}{(2n_V-3)!} \\
&\times \int_0^{1-x} dx_R \frac{(1-x_R-x)^{2n_V-3}}{(1-x_R)^{n_V}} e^{-B_R m_H^2 (x_R - \mu_R)^2}
\end{aligned} \tag{B5}$$

### Appendix C: Valence Spectator's x Integral

In integrating over all momentum fractions of the spectator system we get the following integral as a constant:

$$\begin{aligned}
J_{n_V} &= \int_0^1 dy_2 y_2 \dots \int_0^{1-\sum_{i=2}^{n_V-1} y_i} dy_{n_V} y_{n_V} \delta\left(1-\sum_{i=2}^{n_V} y_i\right) \\
&= \frac{1}{(2n_V-3)!}
\end{aligned} \tag{C1}$$

The last line of Eq. (C1) can be proven with mathematical induction. For the starting case of  $n_V = 2$ ,  $I_2 = 1 = \frac{1}{1!}$ , Now, do the induction step by assuming Eq. (C1) is true up to  $n_V$ . Then,

$$\begin{aligned}
J_{n_V+1} &= \int_0^1 dy_2 y_2 \dots \\
&\times \int_0^{1-\sum_{i=2}^{n_V} y_i} dy_{n_V+1} y_{n_V+1} \delta\left(1-\sum_{i=2}^{n_V+1} y_i\right)
\end{aligned} \tag{C2}$$

For  $i = 3, \dots, n_V + 1$  we change the variables to the relative momentum fraction in the  $3, \dots, n_V + 1$  system:

$$z_i = \frac{y_i}{\sum_{j=3}^{n_V+1} y_j} = \frac{y_i}{1-y_2} \tag{C3}$$

Then, using the relation in Eq. C2

$$\begin{aligned}
J_{n_V+1} &= \int_0^1 dy_2 y_2 (1-y_2)^{2(n_V-2)} J_{n_V} \\
&= \frac{1}{(2n_V-3)!} \int_0^1 dy_2 y_2 (1-y_2)^{2(n_V-2)}.
\end{aligned} \tag{C4}$$

The integral can be taken in terms of the Beta function,  $B(m, n)$ , which in turn can be expressed in terms of factorials since its arguments are integers,

$$\begin{aligned}
\int_0^1 dy_2 y_2 (1-y_2)^{2(n_V-2)} &= B(2, 2n_V-3) \\
&= \frac{1!(2n_V-2-1)!}{(2n_V-1)!}.
\end{aligned} \tag{C5}$$

Thus, using Eq. (C5) in Eq. (C4), one obtains:

$$\begin{aligned}
J_{n_V+1} &= \frac{1}{(2n_V-3)!} \frac{1!(2n_V-2-1)!}{(2n_V-1)!} \\
&= \frac{1}{(2n_V-1)!}
\end{aligned} \tag{C6}$$

and Eq. (C1) holds.

### Appendix D: Numerical Investigation of x Peaking Approximation and Upper Limit

Using the saddle point approximation in Eq. (30), an approximation to the x peak,  $x_p$ , of the PDF was found to be:

$$x_p^{(sp)} = \frac{1}{2(n_V-1)} \left(1 - \frac{m_R}{m_H}\right). \tag{D1}$$

From this we inferred that:

$$x_p \leq \frac{1}{2(n_V-1)}. \tag{D2}$$

Here we explore the validity of the above approximation numerically by looking at the cases of  $n_V = 2, 3, 4$  and  $B_R m_H^2 = 10, 45, 80$ , the latter values being typical when the model was applied to the case of the proton [12].

Fig. 5 shows how the peak varies with the mass ratio,  $\frac{m_R}{m_H}$ . The  $x_p$  value was found numerically, using the `scipy.optimize` Python library. It is interesting that for the above plots  $x_p^{(sp)}$  qualitatively matches  $x_p$  well, monotonically decreasing with  $m_R/m_H$  and being nearly linear. Also, in all cases investigated the upper limit  $x_p \leq \frac{1}{2(n_V-1)}$  held.



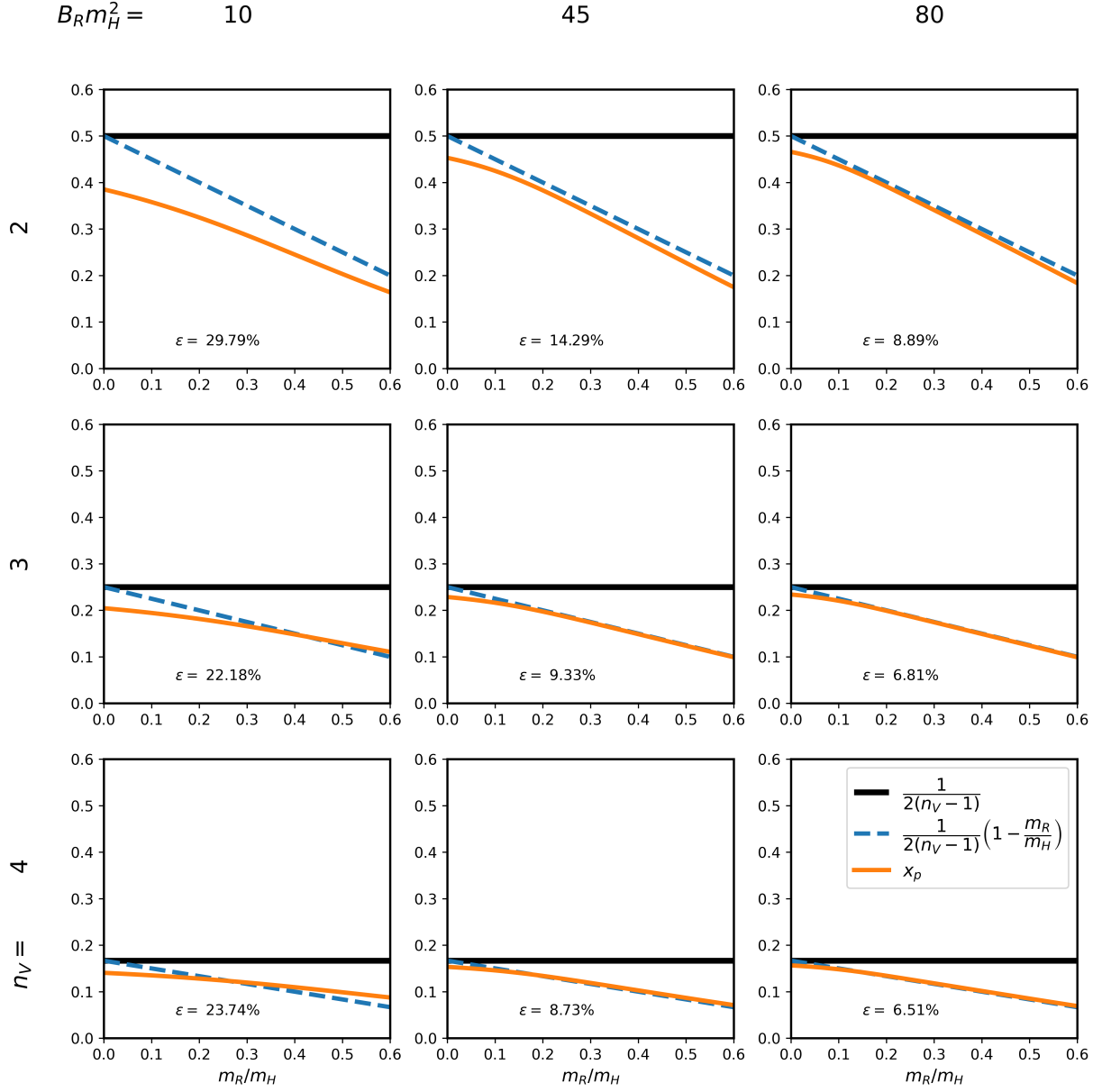


FIG. 5: A comparison of  $x_p$  with the approximation in Eq. 32 for various configurations and with a mass ratio range of  $0 < m_R/m_H < 0.6$ . The  $\epsilon$  displayed represents the largest relative error of the approximation found for the given configuration.